BiOCl and g-C3N4

Subjects: Others

Contributor: Qiang Ren

Many organic pollutants are discharged into the environment, which results in the frequent detection of organic pollutants in surface water and underground water. Some of the organic pollutants can stay for a long time in the environment due to their recalcitrance. Advanced oxidation processes (AOPs) can effectively treat the recalcitrant organic compounds in water. Photocatalysis as one of the AOPs has attracted a lot of interest. BiOCl and g-C3N4 are nice photocatalysts. However, their catalytic activity should be further improved for industrial utilization. The construction of heterojunction between the two different components is deemed as an efficient strategy for developing a highly efficient photocatalyst. As a typical type-II heterojunction, g-C3N4/BiOCl heterojunctions showed better photocatalytic performance. To date, the g-C3N4/BiOCl composites were mainly studied in the field of water purification. The photoactivity of the pristine catalysts was greatly enhanced by the combination of the two materials. However, three kinds of proposed mechanisms were used to explain the improvement of the g-C3N4/BiOCl heterojunctions. But few researchers tried to explain why there were three different scenarios employed to explain the charge transfer. According to the articles reviewed, no direct evidence could indicate whether the band structures of the heterojunctions based on BiOCl and g-C3N4 were changed. Therefore, many more studies are needed to reveal the truth. Having a clearer understanding of the mechanism is beneficial for researchers to construct more efficient photocatalysts. This article is trying to start a new direction of research to inspire more researchers to prepare highly effective photocatalysts.

BiOCl C3N4 photocatalysis mechanism

1. Introduction

With the development of human civilization, many refractory pollutants were discharged to the environment, which are hard to be degraded by traditional purification methods. For example, pollutants like tetracycline [1], bisphenol A [2], Astrazone Black [3], estriol [4], and tetraethylated rhodamine [5] can hardly be degraded by normal waste-water treatment plants. Generally, the degradation of recalcitrant organic pollutants relies on the consumption of energy, such as the Fenton process. Photocatalysis has drawn much attention because of the utilization of solar energy and friendliness to the environment.

In photocatalysis, the heterojunction of two different materials is deemed as an efficient strategy to develop diverse hybrid composites with multiple functionalities [6]. Photocatalysts normally possess some defects that restrict the utilization of the material, for example, ultrafast recombination of photo-induced charge carriers [7], low efficient utilization of sunlight, and wide bandgap [8]. Hybridization of two different catalysts would be an excellent way to improve the photoactivity. Lots of photocatalysts were synthesized in order to enhance the photoactivity of the

catalysts, such as MoS_2/g-C_3N_4 [9], $CuInS_2$/g-C_3N_4 [10], Ag_2O/g-C_3N_4 [11], Ag_2O/TiO_2 [12], $AgI/CuBi_2O_4$ [13], $CuS/BiVO_4$ [14], Ag_3PO_4/MoS_2 [15], g-C_3N_4/SiO_2 [16], $ZnFe_2O_4/TiO_2$ [17], $LaFeO_3/SnS_2$ [18], Bi_2O_3/g-C_3N_4 [19], and Ag_2O/Bi_5O_7I [20]. Recently, heterojunctions based on BiOCl and g-C_3N_4 drew much attention because of the abundance of the materials in the environment.

Graphitic carbon nitride is regarded as a nice photocatalyst because of its nontoxicity, stability in pH over a broad range (0–14), easy to prepare, and the narrow bandgap [21]. After being first synthesized in 1834 [22], carbon nitride has been used in many areas, such as virus inactivation [23], activation of benzene [24], H_2 revolution [25][26], fuel cells [27], CO_2 reduction [28], and organic pollutants degradation [29]. However, because of its high recombination rate of the photogenerated charge carriers and low BET surface area, the application of g-C_3N_4 is restricted. Recently, many studies focused on building heterojunctions to improve its photoactivity, such as the system of WO_3/g-C_3N_4 [30], $ZnWO_4$/g-C_3N_4 [31], and In_2S_3/g-C_3N_4 [32]. According to these studies, coupling graphitic carbon nitride with other kinds of semiconductors could construct better photocatalysts by reducing the recombination rate of the photogenerated charge carriers or increasing the surface area.

On the contrary, layered structure of BiOCl facilitates the photogenerated charge carriers' separation and endows it with a strong ability to degrade organic pollutants [33]. Morphology control was employed by many researchers to improve the pristine catalyst [34]. For example, according to E. Ramírez Meneses and co-workers [35], the addition of capping agents could affect the morphology of BiOCl. However, the as-prepared catalysts were unable to be excited by visible light. In order to expand the light absorption range of BiOCl, many researchers synthesized heterostructures like carbon dots/BiOCl [36], BiOCl/g-C_3N_4 [37], WO_3/BiOCl [38], Bi_2MoO_6-BiOCl [33], BiOCl/BiOBr [39], m-Bi_2O_4/BiOCl [40], $BiOCl/BiVO_4$ [41], $Bi_2O_2CO_3$/BiOCl [42], and BiOI/BiOCl [43].

Among them, the composition of BiOCl and g-C_3N_4 is considered as an excellent combination. The heterojunction could enhance the separation of the photo-induced charge carriers and enable the catalyst to respond to visible light [43][44]. Noble metal doping is also considered as a good method to improve the semiconductor. However, the high cost of noble metal doping restricts its utilization. If a noble metal doping catalyst is used repeatedly, the catalyst will be eroded, and perhaps generate new pollutants [45]. Heterojunctions of semiconductors is friendly to the environment, stable, and abundant in nature. Especially, the system of g-C_3N_4/BiOCl could be used repeatedly and facile to be produced.

Some researchers also found the photoactivity of g-C_3N_4/BiOCl heterojunctions could be further enhanced by combining them with other materials. For example, the systems of Bi_2S_3/BiOCl/g-C_3N_4 [46], BiOCl/g-C_3N_4/kaolinite [47], and g-C_3N_4/CDs (carbon dots)/BiOCl [48]. Notably, through the addition of mediators, Z-scheme catalysts can be synthesized, such as the systems of g-C_3N_4/Au/BiOCl [49] and BiOCl/RGO/protonated g-C_3N_4 [50]. However, few researchers have focused on figuring out which method could prompt the photoactivity of the binary heterojunction. According to all the articles reviewed here, analysis of the proposed mechanism was an important section. Based on the adopted characterizations and experiments, the mechanism was discussed to help readers to understand the whole photocatalysis process.

2. Mechanisms of the BiOCl/g-C_3N_4 Heterojunctions

P-type photocatalyst BiOCl combined with typical n-type photocatalyst g-C_3N_4 could form a conventional type-II photocatalyst with a staggered-gap band structure. There are three different types of semiconductor heterojunctions overall as shown in **Figure 1**. In a type-I heterojunction, conduction band (CB) and valence band (VB) of the semiconductor (SC1) are higher and lower than that of the other semiconductor (SC2), respectively. When SC1 and SC2 construct type-II heterojunction, CB and VB of SC1 are higher than of SC2. Because of the built-in electric field formed inside of the composite, photo-induced electrons tend to migrate to the CB of SC2. At the same time, holes accumulate on VB of SC1 rapidly. Because the electrons and holes migrate to different semiconductors, charge separation is enhanced. The pattern of charge carriers' movement in type-III heterojunction is the same as in type-II heterojunction. The difference of the band structures of the two semiconductors is even larger than in the type-II heterojunction [51].

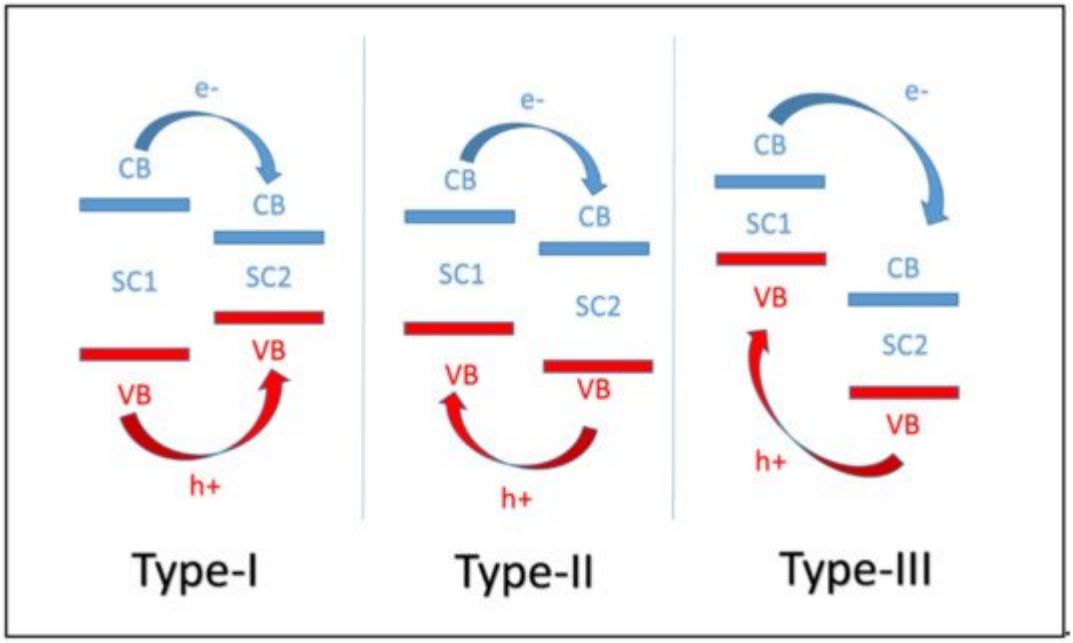

Figure 1. Three different types of semiconductor heterojunction.

Separation of electron-hole pairs could be prompted by the construction of the g-C_3N_4/BiOCl heterojunction. Solar energy utilization of the heterojunction was also more efficient since the wavelength of photo-response was broadened [8]. According to the articles reviewed, an interesting phenomenon is observed, some researchers believed that band structures of the two catalysts stayed unchanged after the combination of the two materials, whereas others thought that CB and VB of g-C_3N_4/BiOCl changed to align Fermi energy levels.

Theoretically, the Fermi energy level of an n-type catalyst is close to the bottom of CB. The Fermi energy level of a p-type catalysts is close to the top of VB [52]. After construction of heterojunction, the CB and VB of n-type catalyst tend to move downward, while those of p-type catalyst are moving upward. This kind of heterojunction based on g-

C_3N_4 and BiOCl is labeled as PCNB in this article. The CB and VB of some g-C_3N_4/BiOCl heterojunctions stayed the same after the combination. This kind of heterojunction is denoted as the system of CNB here.

2.1. CNB Heterojunction

Generally, the proposed mechanism for the generation of reactive radicals on the surface of CNB heterojunction is shown in **Figure 2**. Photoexcited electrons firstly generated in the conduction band of g-C_3N_4 by irradiation of visible light because of its relatively mild band gap (2.7 eV). When it comes to dye degradation, photo-induced charge carriers also generated through dye sensitization. Then, electrons transferred to the conduction band of BiOCl because the conduction band of BiOCl is less negative than that of g-C_3N_4. Photogenerated electrons tend to transfer to a less negative conduction band. Electrons could react with O_2 on the surface of CNB to generate superoxide radicals. At the same time, holes remaining in the valence band of g-C_3N_4 react with surface-absorbed H_2O to generate hydroxyl radicals, so that separation of photo-generated charge carriers is improved and the catalyst can response to visible light. However, the redox ability of the heterojunction was sacrificed when photoactivity is improved, because the holes accumulated on VB of g-C_3N_4.

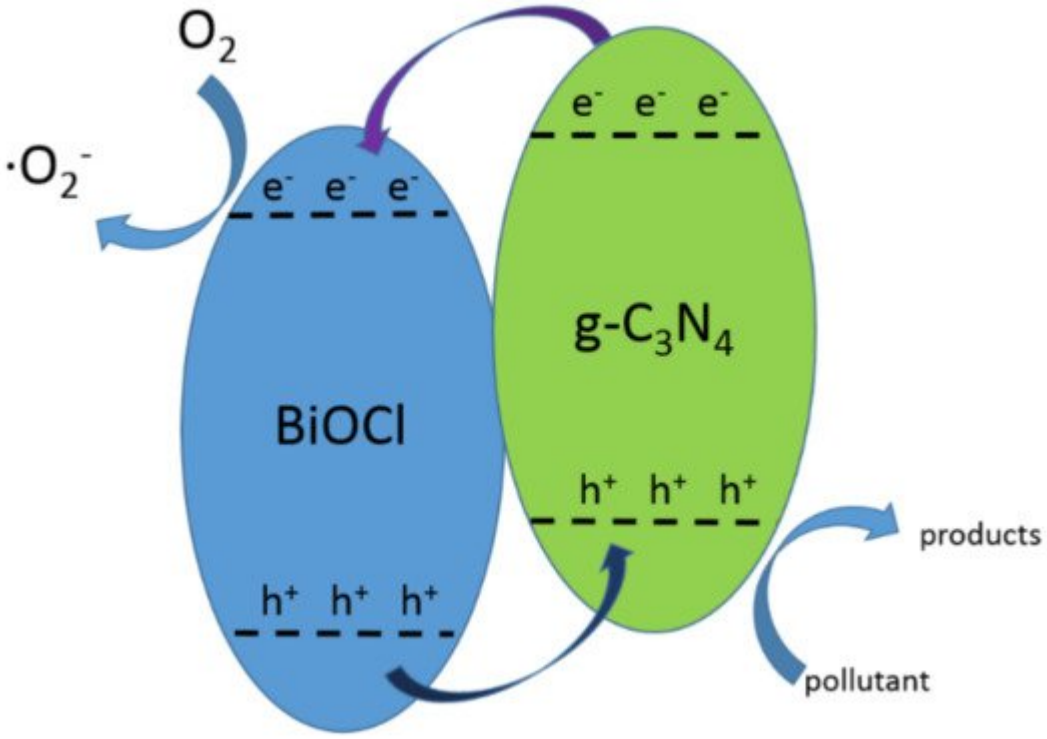

Figure 2. The mechanism for the generation of reactive radicals over CNB.

The mechanism mentioned above was adopted by Faisal Al Marzouqi and co-workers to explain the degradation of nizatidine over the BiOCl/g-C_3N_4 heterojunction [53]. The degradation efficiency of nizatidine was improved under the irradiation of visible light. According to the XRD pattern, the as-prepared catalyst was constructed by pure BiOCl and g-C_3N_4. The construction of the heterojunction was verified. As shown in the UV-vis diffuse reflectance

spectra, the absorption edge of BiOCl was about 364 nm (in the UV range), and that of g-C_3N_4 was about 450 nm (in the visible range). After being combined, the absorption band edge of the heterojunction could be up to 476 nm. The photoactivity of the heterojunction was improved. The bandgap value for 10% BiOCl/g-C_3N_4 sample was 2.6 eV, which endowed the catalyst with the highest photoactivity among all the as-prepared samples. Therefore, the bandgap of the composite was narrowed by combination of the two components. The degradation rate of nizatidine was enhanced by the construction of the heterojunction as shown in **Figure 3**b. This improvement was explained by the double-charge transfer mechanism as proposed in **Figure 2**. Obviously, the CB and VB of both pristine catalysts did not change. The generation of reactive radicals depicted in the article was the same as that in **Figure 2**. However, the article provided no further evidence to prove the main reactive radicals. The presence of hydroxyl radicals was supposed to be the main cause of the degradation of nizatidine in the article. But the study did not exclude the possibility that the hydroxyl radicals could be generated from superoxide radicals. Y. Yang and colleagues demonstrated hydroxyl and superoxide radicals were the main species during the photocatalytic oxidation of MB, too [54]. Hydroxyl radicals were supposed to be produced in the VB of g-C_3N_4.

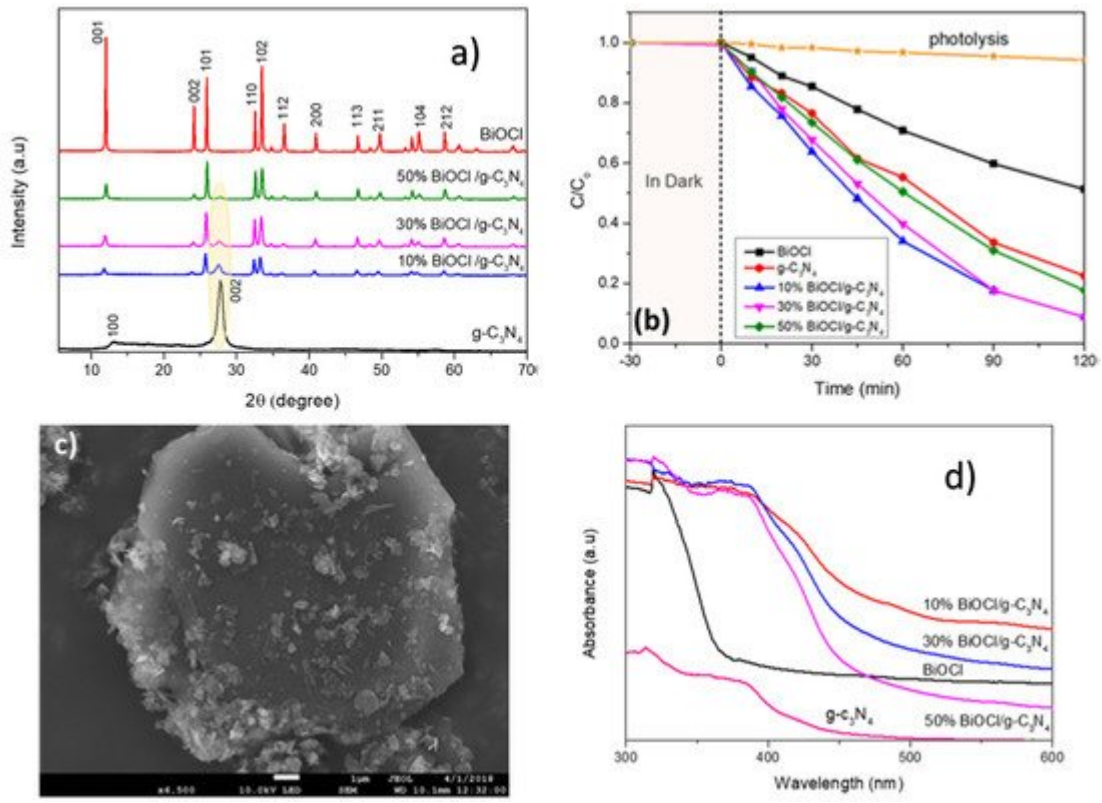

Figure 3. (**a**) XPR pattern of as-prepared BiOCl/g-C_3N_4 samples; (**b**) Degradation rate of nizatidine at an initial concentration of 5 mg/L and pH = 5.6 with all the prepared samples; (**c**) SEM image of 10% BiOCl/g-C_3N_4 sample; (**d**) UV-vis diffuse reflectance spectra of the obtained samples. Reproduced with permission from Al Marzouqi F et al, ACS Omega; published by American Chemical Society, 2013.

To date, lots of CNB heterojunctions were reported. Wenwen Liu and colleagues constructed a 2-dimensional layered BiOCl/g-C_3N_4 composite, and the photodegradation of MO was greatly improved through constructing a CNB heterojunction [55]. When the mass ratio of BiOCl reached 70%, BiOCl/g-C_3N_4 heterojunction showed the

highest photocatalytic performance. EIS images and PL spectra were carried out to prove that better charge separation was realized. The proposed mechanism was similar to that shown in **Figure 2**. Electrons generated in the conduction band of g-C_3N_4, and then transferred to the conduction band of BiOCl. As a result, superoxide radicals generated on the surface of the heterojunction. Holes in the valence band of C_3N_4 were accumulated to participate in the degradation of MO degradation. Trapping experiments exhibited $\bullet O_2^-$ and holes were the main reactive species in the degradation of MO, which could be the evidence of the proposed mechanism. In this study, the VB and CB positions of BiOCl and g-C_3N_4 were determined by the Mott-Schottky curve. The alignment of band edges during the combination of the two materials was not taken into consideration, though the researchers did not directly adopt the standard values. The presence of the main reactive species was consistent with the proposed mechanism. Liwen Lei and co-workers prepared another heterostructure photocatalyst by combining BiOCl and g-C_3N_4 [34]. Arabic gum (AG) was added while synthesizing the heterojunction. They also proved that the superoxide and holes are the main reactive species through trapping experiments. The mechanism shown in **Figure 2** was also adopted to explain the degradation of RhB over the composite.

However, the BiOCl/g-C_3N4 heterojunction prepared by Xiaojing Wang and colleagues showed a different result [44]. Like the studies mentioned above [55], XPR, FT-IR spectroscopy, and PL emission spectra were carried out to demonstrate the formation of the heterojunction. The light response wavelength of BiOCl was broadened, while the charge separation was enhanced. Trapping experiments were also carried out to detect the main reactive species in the photocatalytic process. It turned out that $\bullet O_2^-$ was not the main reactive species, whereas holes played an important role during the degradation of MO.

Why the hydroxyl radicals were not generally supposed to generate during the photocatalytic reaction was not mentioned in the above studies. Zhang Sai and co-workers explained the reason in their study [56], the standard CB and VB potentials of g-C_3N_4 are approximately −1.3 and 1.40 eV, respectively. The standard redox potential of $\bullet O_2^-/O_2$ is −0.13 eV (vs. NHE), which is more positive than the CB potential of g-C_3N_4. So, it is very easy for e- on the CB of g-C_3N_4 to generate superoxide radicals. The VB potential of g-C_3N_4 is less positive than the standard potential of $\bullet OH/OH^-$, which is +1.99 eV (vs. NHE). This makes holes on the VB of the catalyst and cannot be captured and to produce •OH radicals. If the CB and VB of the g-C_3N_4/BiOCl catalysts stay unchanged after the construction of the type-II heterojunction, electrons accumulate on the CB of BiOCl (−1.1 eV) [8] to form $\bullet O_2^-$. Holes migrate to the VB of g-C_3N_4, but cannot generate hydroxyl radicals. Therefore, superoxide radicals and holes are the main reactive species in the systems of BiOCl/g-C_3N_4. This theory is consistent with the results mentioned above. The work of L. Song and co-workers also suggested that the standard redox potential of the VB of g-C_3N_4 was not positive enough to generate •OH groups [57]. J. Sun and colleagues directly used the standard potentials of the pristine catalysts to describe the mechanism without taking the alignment of the Fermi energy level into account [58].

Q. Li and co-workers employed the result of X-ray photoelectron spectroscopy (VB XPS) spectra to determine the VB of pure g-C_3N_4, which was 1.44 eV NHE [59]. Compared to the standard potential of $\bullet OH/OH^-$, the generation of •OH was not expected to happen on the VB of g-C_3N_4. The result of trapping experiments suggested that $\bullet O_2^-$ and holes were the dominant reactive species during the degradation of MO.

Some other researchers did not only adopt trapping experiments to determine the main species, for example, L. Song and co-workers also adopted ESR spectra and trapping experiments to find out the main reactive species [60]. The presence of superoxide radicals was directly proved by the ESR test. The generation of hydroxyl radicals was not detected. Trapping experiments proved holes also played an important role during the oxidation of RhB.

Just like the aforementioned study of Xiaojing Wang and colleagues [44], T. Jia and colleagues determined the CB and VB potentials of BiOCl and g-C_3N_4 by using theoretical calculation, then holes were proved to be the main reactive species during the oxidation of MB through trapping experiments [61].

There are some other studies that adopted a similar mechanism to explain the degradation of pollutants over ternary catalysts based on the system of BiOCl/g-C_3N_4, like systems of BiOCl/g-C_3N_4/kaolinite [47], g-C_3N_4/CDs/BiOCl [48], BiOCl/CdS/g-C_3N_4 [62], and BiOI-BiOCl/C_3N_4 [63].

However, Xiaojuan Bai and colleagues demonstrated that hydroxyl radicals were still produced, though the VB of g-C_3N_4 was not positive enough [64]. They synthesized a kind of photocatalyst by modifying g-C_3N_4 with fullerene. After the modification, the degradation rate of MB was improved. Trapping and ESR experiments proved that holes and •OH were the main reactive species in the photodegradation of MB. After the modification, the VB of C_{60}/g-C_3N_4 was more positive by 0.17 eV. Considering the theory depicted above, that was not positive enough to generate •OH directly on the VB of g-C_3N_4. The mechanism was further researched by adding N_2 to create an anoxic suspension. The degradation of MB was almost unchanged in the presence of N_2, which indicated that the •OH was generated on the surface of the composite, but not through the reaction induced by electrons on the CB of g-C_3N_4. This study seems contradictory to the theory described above that the VB of g-C_3N_4 was not positive enough to produce •OH [56].

The CNB system is a typical type-II heterojunction due to the band structures of the two materials. Trapping experiments were carried out to clarify the main reactive species, which proved to be superoxide radicals and holes. However, according to the study discussed above [56], there is still something unclear about the mechanism depicted in this section. Some more works are required to elucidate the reaction that happened over the heterojunction of CNB.

References

1. Pan, M.; Wong, C.K.C.; Chu, L.M. Distribution of Antibiotics in Wastewater-Irrigated Soils and Their Accumulation in Vegetable Crops in the Pearl River Delta, Southern China. J. Agric. Food Chem. 2014, 62, 11062–11069.
2. Sharma, V.; Anquandah, G.A.K.; Yngard, R.A.; Kim, H.; Fekete, J.; Bouzek, K.; Ray, A.K.; Golovko, D. Nonylphenol, octylphenol, and bisphenol-A in the aquatic environment: A review on occurrence, fate, and treatment. J. Environ. Sci. Health Part A 2009, 44, 423–442.

3. Yesilada, O.; Asma, D.; Cing, S. Decolorization of textile dyes by fungal pellets. Process. Biochem. 2003, 38, 933–938.
4. Ahern, J.; Fairchild, R.; Thomas, J.S.; Carr, J.; Patterson, H.H. Characterization of BiOX compounds as photocatalysts for the degradation of pharmaceuticals in water. Appl. Catal. B Environ. 2015, 179, 229–238.
5. Sun, S.; Wang, W.; Zhang, L.; Zhou, L.; Yin, W.; Shang, M. Visible Light-Induced Efficient Contaminant Removal by Bi5O7I. Environ. Sci. Technol. 2009, 43, 2005–2010.
6. Chang, F.; Xie, Y.; Zhang, J.; Chen, J.; Li, C.; Wang, J.; Luo, J.; Deng, B.; Hu, X. Construction of exfoliated g-C3N4 nanosheets–BiOCl hybrids with enhanced photocatalytic performance. RSC Adv. 2014, 4, 28519–28528.
7. Zhou, C.; Lai, C.; Xu, P.; Zeng, G.; Huang, D.; Li, Z.; Zhang, C.; Cheng, M.; Hu, L.; Wan, J.; et al. Rational Design of Carbon-Doped Carbon Nitride/Bi12O17Cl2 Composites: A Promising Candidate Photocatalyst for Boosting Visible-Light-Driven Photocatalytic Degradation of Tetracycline. ACS Sustain. Chem. Eng. 2018, 6, 6941–6949.
8. Yang, Y.; Zhang, C.; Lai, C.; Zeng, G.; Huang, D.; Cheng, M.; Wang, J.; Chen, F.; Zhou, C.; Xiong, W. BiOX (X = Cl, Br, I) photocatalytic nanomaterials: Applications for fuels and environmental management. Adv. Colloid Interface Sci. 2018, 254, 76–93.
9. Liu, Y.; Zhang, H.; Ke, J.; Zhang, J.; Tian, W.; Xu, X.; Duan, X.; Sun, P.H.; Tade, M.; Wang, S. 0D (MoS2)/2D (g-C3N4) heterojunctions in Z-scheme for enhanced photocatalytic and electrochemical hydrogen evolution. Appl. Catal. B Environ. 2018, 228, 64–74.
10. Guo, F.; Shi, W.; Li, M.; Shi, Y.; Wen, H. 2D/2D Z-scheme heterojunction of CuInS2/g-C3N4 for enhanced visible-light-driven photocatalytic activity towards the degradation of tetracycline. Sep. Purif. Technol. 2019, 210, 608–615.
11. Liang, S.; Zhang, D.; Pu, X.; Yao, X.; Han, R.; Yin, J.; Ren, X. A novel Ag2O/g-C3N4 p-n heterojunction photocatalysts with enhanced visible and near-infrared light activity. Sep. Purif. Technol. 2019, 210, 786–797.
12. Liu, G.; Wang, G.; Hu, Z.; Su, Y.; Zhao, L. Ag2O nanoparticles decorated TiO2 nanofibers as a p-n heterojunction for enhanced photocatalytic decomposition of RhB under visible light irradiation. Appl. Surf. Sci. 2019, 465, 902–910.
13. Guo, F.; Shi, W.; Wang, H.; Han, M.; Guan, W.; Huang, H.; Liu, Y.; Kang, Z. Study on highly enhanced photocatalytic tetracycline degradation of type II AgI/CuBi2O4 and Z-scheme AgBr/CuBi2O4 heterojunction photocatalysts. J. Hazard. Mater. 2018, 349, 111–118.
14. Lai, C.; Zhang, M.; Li, B.; Huang, D.; Zeng, G.; Qin, L.; Liu, X.; Yi, H.; Cheng, M.; Li, L.; et al. Fabrication of CuS/BiVO4 (0 4 0) binary heterojunction photocatalysts with enhanced

photocatalytic activity for Ciprofloxacin degradation and mechanism insight. Chem. Eng. J. 2019, 358, 891–902.

15. Zhu, C.; Zhang, L.; Jiang, B.; Zheng, J.; Hu, P.; Li, S.; Wu, M.; Wu, W. Fabrication of Z-scheme Ag3PO4/MoS2 composites with enhanced photocatalytic activity and stability for organic pollutant degradation. Appl. Surf. Sci. 2016, 377, 99–108.
16. Hao, Q.; Niu, X.; Nie, C.; Hao, S.; Zou, W.; Ge, J.; Chen, D.; Yao, W. A highly efficient g-C3N4/SiO2 heterojunction: The role of SiO2 in the enhancement of visible light photocatalytic activity. Phys. Chem. Chem. Phys. 2016, 18, 31410–31418.
17. Nguyen, T.B.; Huang, C.; Doong, R.-A. Photocatalytic degradation of bisphenol A over a ZnFe2O4/TiO2 nanocomposite under visible light. Sci. Total Environ. 2019, 646, 745–756.
18. Luo, J.; Li, R.; Chen, Y.; Zhou, X.; Ning, X.; Zhan, L.; Ma, L.; Xu, X.; Xu, L.; Zhang, L. Rational design of Z-scheme LaFeO3/SnS2 hybrid with boosted visible light photocatalytic activity towards tetracycline degradation. Sep. Purif. Technol. 2019, 210, 417–430.
19. He, R.; Zhou, J.; Fu, H.; Zhang, S.; Jiang, C. Room-temperature in situ fabrication of Bi2O3/g-C3N4 direct Z-scheme photocatalyst with enhanced photocatalytic activity. Appl. Surf. Sci. 2018, 430, 273–282.
20. Chen, Y.; Zhu, G.; Hojamberdiev, M.; Gao, J.; Zhu, R.; Wang, C.; Wei, X.; Liu, P. Three-dimensional Ag2O/Bi5O7I p–n heterojunction photocatalyst harnessing UV–vis–NIR broad spectrum for photodegradation of organic pollutants. J. Hazard. Mater. 2018, 344, 42–54.
21. Shi, S.; Gondal, M.; Al-Saadi, A.; Fajgar, R.; Kupcik, J.; Chang, X.; Shen, K.; Xu, Q.; Seddigi, Z. Facile preparation of g-C3N4 modified BiOCl hybrid photocatalyst and vital role of frontier orbital energy levels of model compounds in photoactivity enhancement. J. Colloid Interface Sci. 2014, 416, 212–219.
22. Ong, W.-J.; Tan, L.-L.; Ng, Y.H.; Yong, S.-T.; Chai, S.-P. Graphitic Carbon Nitride (g-C3N4)-Based Photocatalysts for Artificial Photosynthesis and Environmental Remediation: Are We a Step Closer to Achieving Sustainability? Chem. Rev. 2016, 116, 7159–7329.
23. Li, Y.; Zhang, C.; Shuai, D.; Naraginti, S.; Wang, D.; Zhang, W. Visible-light-driven photocatalytic inactivation of MS2 by metal-free g-C3N4: Virucidal performance and mechanism. Water Res. 2016, 106, 249–258.
24. Goettmann, F.; Fischer, A.; Antonietti, M.; Thomas, A. Metal-free catalysis of sustainable Friedel–Crafts reactions: Direct activation of benzene by carbon nitrides to avoid the use of metal chlorides and halogenated compounds. Chem. Commun. 2006, 4530–4532.
25. Wang, X.; Maeda, K.; Thomas, A.; Takanabe, K.; Xin, G.; Carlsson, J.M.; Domen, K.; Antonietti, M. A metal-free polymeric photocatalyst for hydrogen production from water under visible light. Nat. Mater. 2009, 8, 76–80.

26. Liu, J.; Liu, Y.; Liu, N.; Han, Y.; Zhang, X.; Huang, H.; Lifshitz, Y.; Lee, S.-T.; Zhong, J.; Kang, Z. Metal-free efficient photocatalyst for stable visible water splitting via a two-electron pathway. Science 2015, 347, 970–974.
27. Zheng, Y.; Liu, J.; Liang, J.; Jaroniec, M.; Qiao, S.Z. Graphitic carbon nitride materials: Controllable synthesis and applications in fuel cells and photocatalysis. Energy Environ. Sci. 2012, 5, 6717–6731.
28. Pawar, R.; Kang, S.; Ahn, S.H.; Lee, C.S. Gold nanoparticle modified graphitic carbon nitride/multi-walled carbon nanotube (g-C3N4/CNTs/Au) hybrid photocatalysts for effective water splitting and degradation. RSC Adv. 2015, 5, 24281–24292.
29. Lan, M.; Fan, G.; Yang, L.; Li, F. Enhanced visible-light-induced photocatalytic performance of a novel ternary semiconductor coupling system based on hybrid Zn–In mixed metal oxide/g-C3N4 composites. RSC Adv. 2014, 5, 5725–5734.
30. Huang, L.; Xu, H.; Li, Y.; Li, H.; Cheng, X.; Xia, J.; Xu, Y.; Cai, G. Visible-light-induced WO3/g-C3N4 composites with enhanced photocatalytic activity. Dalton Trans. 2013, 42, 8606–8616.
31. Wang, Y.; Wang, Z.; Muhammad, S.; He, J. Graphite-like C3N4 hybridized ZnWO4 nanorods: Synthesis and its enhanced photocatalysis in visible light. CrystEngComm 2012, 14, 5065–5070.
32. Xing, C.; Wu, Z.; Jiang, D.; Chen, M. Hydrothermal synthesis of In2S3/g-C3N4 heterojunctions with enhanced photocatalytic activity. J. Colloid Interface Sci. 2014, 433, 9–15.
33. Han, G.; Li, D.Y.; Zheng, Y.F.; Song, X.C. Enhanced Visible-Light-Responsive Photocatalytic Properties of Bi2MoO6-BiOCl Nanoplate Composites. J. Nanosci. Nanotechnol. 2018, 18, 5575–5581.
34. Lei, L.; Gao, D.; Jin, H.; Zhang, Q.; Xu, J.; Fu, Z. A novel enhanced visible-light-driven photocatalyst via hybridization of nanosized BiOCl and graphitic C3N4. Dalton Trans. 2015, 44, 795–803.
35. Ramírez-Meneses, E.; Valencia-Barrón, J.P.; Hernández-Pérez, M.A.; Domínguez-Crespo, M.A.; Torres, A.; Palacios, E. Synthesis and Characterization of BiOCl Powders with Soft Templates. J. Inorg. Organomet. Polym. Mater. 2018, 28, 2350–2364.
36. Lin, W.; Yu, X.; Shen, Y.; Chen, H.; Zhu, Y.; Zhang, Y.; Meng, H. Carbon dots/BiOCl films with enhanced visible light photocatalytic performance. J. Nanoparticle Res. 2017, 19, 56.
37. Singh, S.; Sharma, R.; Khanuja, M. A review and recent developments on strategies to improve the photocatalytic elimination of organic dye pollutants by BiOX (X=Cl, Br, I, F) nanostructures. Korean J. Chem. Eng. 2018, 35, 1955–1968.
38. Yu, C.L.; Chen, J.C.; Zhou, W.Q.; Wei, L.F.; Fan, Q.Z. Grinding calcination preparation of WO3/BiOCl heterostructures with enhanced visible light photocatalytic activity. Mater. Res. Innov.

2014, 19, 54–59.

39. Cui, Z.; Song, H.; Ge, S.; He, W.; Liu, Y. Fabrication of BiOCl/BiOBr hybrid nanosheets with enhanced superoxide radical dominating visible light driven photocatalytic activity. Appl. Surf. Sci. 2019, 467, 505–513.
40. Junxiu, W.; Zhenzong, Z.; Xi, W.; Yi, S.; Yongfu, G.; Keung, W.P.; Renbi, B. Synthesis of novel p-n heterojunction m-Bi2O4/BiOCl nanocomposite with excellent photocatalytic activity through ion-etching method. Chin. J. Catal. 2018, 39, 1792–1803.
41. Song, L.; Pang, Y.; Zheng, Y.; Chen, C.; Ge, L. Design, preparation and enhanced photocatalytic activity of porous BiOCl/BiVO4 microspheres via a coprecipitation-hydrothermal method. J. Alloys Compd. 2017, 710, 375–382.
42. Yu, L.; Zhang, X.; Li, G.; Cao, Y.; Shao, Y.; Li, D. Highly efficient Bi2O2CO3/BiOCl photocatalyst based on heterojunction with enhanced dye-sensitization under visible light. Appl. Catal. B Environ. 2016, 187, 301–309.
43. Zhong, Y.; Liu, Y.; Wu, S.; Zhu, Y.; Chen, H.; Yu, X.; Zhang, Y. Facile Fabrication of BiOI/BiOCl Immobilized Films with Improved Visible Light Photocatalytic Performance. Front. Chem. 2018, 6, 58.
44. Wang, X.J.; Wang, Q.; Li, F.-T.; Yang, W.-Y.; Zhao, Y.; Hao, Y.-J.; Liu, S.-J. Novel BiOCl–C3N4 heterojunction photocatalysts: In situ preparation via an ionic-liquid-assisted solvent-thermal route and their visible-light photocatalytic activities. Chem. Eng. J. 2013, 234, 361–371.
45. Zhang, C.; Li, Y.; Shuai, D.; Shen, Y.; Xiong, W.; Wang, L. Graphitic carbon nitride (g-C3N4)-based photocatalysts for water disinfection and microbial control: A review. Chemosphere 2019, 214, 462–479.
46. Liu, S.; Liu, Y.; Dai, G.; Bao, X.; Huang, N.; Peng, R.; Zhou, Y. Synthesis and characterization of novel Bi2S3/BiOCl/g-C3N4 composite with efficient visible-light photocatalytic activity. Mater. Lett. 2019, 241, 190–193.
47. Dong, X.; Sun, Z.; Zhang, X.; Li, C.; Zheng, S. Construction of BiOCl/g-C3N4/kaolinite composite and its enhanced photocatalysis performance under visible-light irradiation. J. Taiwan Inst. Chem. Eng. 2018, 84, 203–211.
48. Asadzadeh-Khaneghah, S.; Habibi-Yangjeh, A.; Yubuta, K. Novel g-C3N4 nanosheets/CDs/BiOCl photocatalysts with exceptional activity under visible light. J. Am. Ceram. Soc. 2018, 102, 1435–1453.
49. Zhao, S.; Zhang, Y.; Zhou, Y.; Fang, J.; Wang, Y.; Zhang, C.; Chen, W. Fabrication of sandwich-structured g-C3N4/Au/BiOCl Z-scheme photocatalyst with enhanced photocatalytic performance under visible light irradiation. J. Mater. Sci. 2018, 53, 6008–6020.

50. Xue, J.; Li, X.; Ma, S.; Xu, P.; Wang, M.; Ye, Z. Facile fabrication of BiOCl/RGO/protonated g-C3N4 ternary nanocomposite as Z-scheme photocatalyst for tetracycline degradation and benzyl alcohol oxidation. J. Mater. Sci. 2018, 54, 1275–1290.
51. Marschall, R. Semiconductor Composites: Strategies for Enhancing Charge Carrier Separation to Improve Photocatalytic Activity. Adv. Funct. Mater. 2014, 24, 2421–2440.
52. Wang, H.; Zhang, L.; Chen, Z.; Hu, J.; Li, S.; Wang, Z.; Liu, J.; Wang, X. Semiconductor heterojunction photocatalysts: Design, construction, and photocatalytic performances. Chem. Soc. Rev. 2014, 43, 5234–5244.
53. AlMarzouqi, F.; Al Farsi, B.; Kuvarega, A.T.; Al Lawati, H.A.J.; Al Kindy, S.M.Z.; Kim, Y.; Selvaraj, R. Controlled Microwave-Assisted Synthesis of the 2D-BiOCl/2D-g-C3N4 Heterostructure for the Degradation of Amine-Based Pharmaceuticals under Solar Light Illumination. ACS Omega 2019, 4, 4671–4678.
54. Yang, Y.; Zhou, F.; Zhan, S.; Liu, Y.; Yin, Y. Enhanced Photocatalytic Activity of BiOCl Hybridized with g-C3N4. J. Inorg. Organomet. Polym. Mater. 2016, 26, 91–99.
55. Liu, W.; Qiao, L.; Zhu, A.; Liu, Y.; Pan, J. Constructing 2D BiOCl/C3N4 layered composite with large contact surface for visible-light-driven photocatalytic degradation. Appl. Surf. Sci. 2017, 426, 897–905.
56. Zhang, S.; Gu, P.; Ma, R.; Luo, C.; Wen, T.; Zhao, G.; Cheng, W.; Wang, X. Recent developments in fabrication and structure regulation of visible-light-driven g-C3N4-based photocatalysts towards water purification: A critical review. Catal. Today 2019, 335, 65–77.
57. Song, L.; Zheng, Y.; Chen, C. Sonication-assisted deposition–precipitation synthesis of graphitic C3N4/BiOCl heterostructured photocatalysts with enhanced rhodamine B photodegradation activity. J. Mater. Sci. Mater. Electron. 2017, 28, 15861–15869.
58. Sun, J.; Song, J.; Gondal, M.A.; Shi, S.; Lu, Z.; Xu, Q.; Chang, X.; Xiang, D.; Shen, K. Preparation of g-C3N4/BiOX (X = Cl, Br, I) composites, and their photocatalytic activity under visible light irradiation. Res. Chem. Intermed. 2014, 41, 6941–6955.
59. Li, Q.; Zhao, X.; Yang, J.; Jia, C.-J.; Jin, Z.; Fan, W. Exploring the effects of nanocrystal facet orientations in g-C3N4/BiOCl heterostructures on photocatalytic performance. Nanoscale 2015, 7, 18971–18983.
60. Song, L.; Pang, Y.; Zheng, Y.; Ge, L. Hydrothermal synthesis of novel g-C3N4/BiOCl heterostructure nanodiscs for efficient visible light photodegradation of Rhodamine B. Appl. Phys. A 2017, 123, 500.
61. Jia, T.; Li, J.; Long, F.; Fu, F.; Zhao, J.; Deng, Z.; Wang, X.; Zhang, Y. Ultrathin g-C3N4 Nanosheet-Modified BiOCl Hierarchical Flower-Like Plate Heterostructure with Enhanced Photostability and Photocatalytic Performance. Crystals 2017, 7, 266.

62. Bellamkonda, S.; Rao, G.R. Nanojunction-mediated visible light photocatalytic enhancement in heterostructured ternary BiOCl/ CdS/g-C3N4 nanocomposites. Catal. Today 2019, 321–322, 18–25.
63. Aghdam, S.M.; Haghighi, M.; Allahyari, S.; Yosefi, L. Precipitation dispersion of various ratios of BiOI/BiOCl nanocomposite over g-C3N4 for promoted visible light nanophotocatalyst used in removal of acid orange 7 from water. J. Photochem. Photobiol. A Chem. 2017, 338, 201–212.
64. Bai, X.; Wang, L.; Wang, Y.; Yao, W.; Zhu, Y. Enhanced oxidation ability of g-C3N4 photocatalyst via C60 modification. Appl. Catal. B Environ. 2014, 152–153, 262–270.